Characterization of a Josephson Junction Comb Generator

Akim A. Babenko[#$1], Alírio S. Boaventura[#2], Nathan E. Flowers-Jacobs[#3], Justus A. Brevik[#],
Anna E. Fox[#], Dylan F. Williams[#], Zoya Popović[$], Paul D. Dresselhaus[#], Samuel P. Benz[#]

[#]National Institute of Standards and Technology, Boulder, USA

[$]Department of Electrical, Computer, and Energy Engineering, University of Colorado, Boulder, USA

[1]akim.babenko@nist.gov, [2]aliriodejesus.soaresboaventura@nist.gov, [3]nathan.flowers-jacobs@nist.gov

Abstract — We present a new type of microwave frequency combs with a potentially calculable pulse shape. The device is an array of 1500 Josephson junctions (JJs) connected in series along a transmission line. The pulse generation is based on the nonlinearity of the JJs. A large-signal network analyzer and a cryogenic probe station are used to characterize the pulses in the frequency domain up to 50 GHz. We compare the measured data to simulations that use the resistively and capacitively shunted JJ model. The amplitude stability of the demonstrated comb generator is better than 0.5 dB per 0.1 dB input drive variation within the operating range. Finally, we observe qualitative agreement between the measured and simulated power spectrum dependence on the input power, and discuss possible improvements to the system model.

Keywords — Pulse measurements, Josephson junctions, Superconducting microwave devices, Millimeter wave measurements, Superconducting integrated circuits.

I. Introduction

With the development of modern telecommunication systems, there is a high demand for accurate characterization of broadband signals and circuits. Among the most utilized instruments for the analysis of wide-band signals and networks are large-signal network analyzers (LSNAs) [1]. LSNAs provide traceable scattering-parameter, absolute power, and cross-frequency phase measurements.

Currently, a broadband power-meter calibrated using a calorimetric technique provides the traceability for power calibration [2]. For traceable cross-frequency phase calibration, various implementations of comb generators (also referred to as frequency combs) based on semiconductor technology are used, for example split signal pulse generators [3], nonlinear transmission lines [4] and step rocevery diodes [5]. These frequency combs provide stable pulses with rich harmonic content, but the pulse shapes (and therefore frequency content) are not predictable *a priori*. Therefore, comb generators must be calibrated using traceable optical techniques described in detail in [6], where the amplitude and phase stability per 0.1 dB input drive variation was ± 0.6 dB and ± 1.9°, respectively.

In this paper we show the first steps towards creating a comb generator with intrinsically calculable harmonic content that could replace the traceability chain described above. This comb generator is based on Josephson junctions (JJs), which are cryogenically cooled devices made with a thin non-superconducting barrier between two superconductors [7]. When current-biased, a JJ generates pulses with rising and falling edges determined by junction parameters and with a
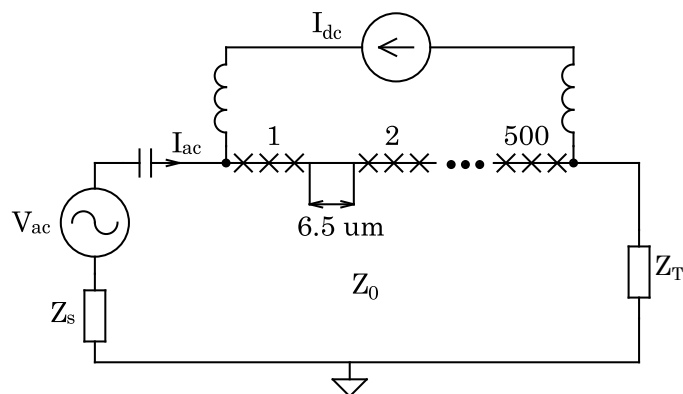

Fig. 1. The diagram of the comb generator. The array of 1500 JJs, placed on a transmission line with the characteristic impedance Z_0, is arranged as 500 stacks with three JJs in each stack. A CW voltage source V_{ac} drives the junctions with the current I_{ac}, in addition to dc bias I_{dc}.

time-integrated voltage across the JJ that is exactly determined by the ratio of defined fundamental constants $h/2e$ (Planck constant and the electron charge). This effect is also utilized for the realization of dc [8] and ac [9] voltage standards. Here we study a Josephson junction comb generator similar to the theoretical proposal in [10], which focused on using pairs of JJs connected in parallel to form SQUIDs (Superconducting Quantum Interference Device) biased using magnetic fields.

An array of JJs connected in series, as in Fig. 1, is biased with a combination of dc and 5 GHz CW current. The harmonic content of the resulting voltage pulses across the junctions is measured up to 50 GHz. The calibration and measurements are performed with a cryogenic probe station [11]. Although the exact knowledge of the integrated area is not sufficient to predict the pulse shape, we use a simple model of the JJ, assuming no parameters variation along the array, as well as the ideal behavior of each of the junctions and a lossless substrate, to calculate the expected harmonic content. We show the agreement between these predictions and calibrated measurements, concentrating on the power spectrum stability of the JJ comb generator versus changes in the drive signal amplitude. We also show the initial results for the phase stability of the JJ comb generator.

II. Pulse Generation Technique

The circuit model of a single JJ with the corresponding calculated time-domain response to a 5 GHz sinusoidal input current is shown in Fig. 2.
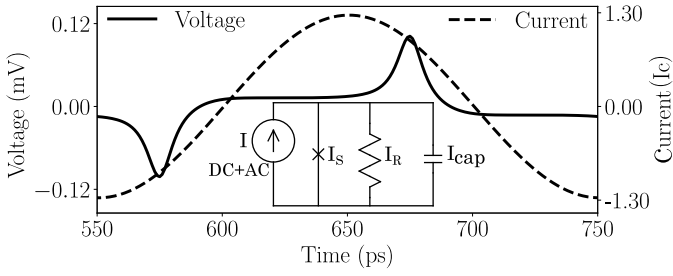
Fig. 2. Simulated time-domain waveforms across a single JJ driven with a 5 GHz CW current. The junction generates pulses with an exact time-integrated voltage area h/2e across the JJ. The pulses are locked to the phase of the drive current.

The dynamics of operation are modeled using the widely-accepted resistively and capacitively shunted junction (RCSJ) equivalent electrical circuit [7], as shown in Fig. 2. The drive current I divides into the superconducting (I_S), resistive (I_R) and capacitive (I_{cap}) currents where $I_{cap} \ll I_R, I_S$ for the technology described below. If the applied current I is below the critical current value, I_C, it flows solely into the superconducting branch and obeys the dc Josephson equation $I = I_S = I_C \sin \phi$, where ϕ is the quantum-mechanical macroscopic phase difference across the JJ [7]. This zero-voltage state corresponds roughly to the flat regions of voltage waveform in Fig. 2. When the input current I exceeds the critical value I_C, a non-zero voltage V evolves across the junction, as given by:

$$I = I_C \sin \phi + V/R_n + C \cdot \partial V/\partial t, \qquad (1)$$

$$\partial \phi/\partial t = (2e/\hbar)V, \qquad (2)$$

where (2) is the ac Josephson equation. Substituting (2) into (1), one obtains a second-order nonlinear differential equation for the phase difference ϕ and solves for V as a function of ϕ. The solution under dc, CW, or pulse drive current $I > I_C$ is of the form of voltage pulses with integrated area equal exactly to $\pm h/2e$. In the dc-only bias case, however, the timing of these pulses is difficult to control and the circuit is sensitive to current noise. Therefore, the voltage pulses are typically generated with a stabilized CW or pulse drive current. An example is shown in Fig. 2, with exactly one pulse per half-period of the CW input drive. The range of bias parameters over which an integer number of output voltage pulses is locked to the input drive is referred to as the Quantum Locking Range (QLR) [9]. The phase shift of the voltage with respect to the drive current stems from (1), and for small input signals $I \ll I_C$ the JJ can be approximated as a non-linear inductor [7]. It is important to note again that the voltage pulses are always phase-locked to the drive current.

When the JJ capacitance C is negligibly small, as in this paper, the –3 dB cutoff frequency is determined as $f_c = I_C R_n (2e/h)$, setting the rising and falling edges of the voltage pulses. Thus, the harmonic content of those voltage pulses is set mainly by the intrinsic properties of the junctions and not by the frequency content of the drive signal, particularly for signals with bandwidth $\ll f_c$. The 0.12 mV amplitude, shown in Fig. 2, was calculated for the JJs in this

paper with measured $I_C R_n = 53 \, \mu\text{V}$ and $f_c = 26 \, \text{GHz}$. From the right y-axis of the plot, one can also see that the amplitude of the 5 GHz drive current should be about 30% above the I_C value to maintain the QLR with exactly one voltage pulse per half-period. The small pulse amplitude across a single JJ is the motivation for connecting thousands of junctions in series to increase the total output voltage.

III. SIMULATION SETUP

We simulated our comb generator using the circuit in Fig. 3 with the WRSpice [12] open-source transient circuit simulator, which includes the RCSJ model of a JJ. The large inductors at the ends of the JJ array are used to both supply a dc current bias to the JJs and to measure the dc and low-frequency content of the voltage pulses. The LSNA CW signal source is modeled as a 5 GHz voltage source with an impedance Z_S that is measured during the calibration procedure described below. The large capacitor is part of the LSNA's dc bias tees. As in Fig. 1, we arrange the series-connected JJs in groups of three that are separated by 6.5 μm along a 50 Ω lossless transmission line. We consider the silicon substrate as a lossless dielectric as our first approximation. The impedance of the termination resistor is determined using a calibrated measurement of a separate on-chip termination structure and is equivalent to a series RL-network with $R_T = 59 \, \Omega$ and $L_T = 96 \, \text{pH}$.

The WRSpice solver solutions are the total voltage V_1 and current I_1 as functions of time at the input node of and through the array, respectively. Those are converted into the peak complex amplitudes of the a_1 and b_1 power waves [13], as shown in Fig. 3 and given by:

$$a_1 = (V_1 + I_1 Z_0)/(2\sqrt{|Z_0|}), \qquad (3)$$

$$b_1 = (V_1 - I_1 Z_0)/(2\sqrt{|Z_0|}), \qquad (4)$$

where Z_0 is equal to 50 Ω. The a_1 wave contains two superimposed components: the incident drive signal component a_1^{inc} and multiple-reflected component a_1^{ref} stemming from the mismatch between the source and the array input impedances. It is conceptually useful to consider the b_1 wave in two different current bias regimes. When the current bias is $I < I_C$, then b_1 contains two distinct components: the linear reflected component due to the impedance mismatch b_1^{mm} and the component b_1^{nl} generated by the small-signal non-linear inductance of the JJs which creates harmonics but not pulses. However, when the current bias is $I > I_C$ then b_1 contains the same impedance mismatch term b_1^{mm} but the
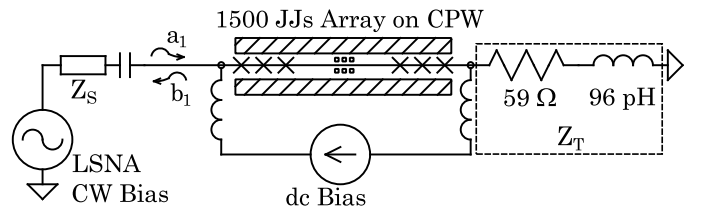

Fig. 3. The circuit used to model the response of the JJ comb generator to a CW drive signal. The values of the source Z_S and termination Z_T impedances are obtained from prior scattering-parameter measurements on the same chip.
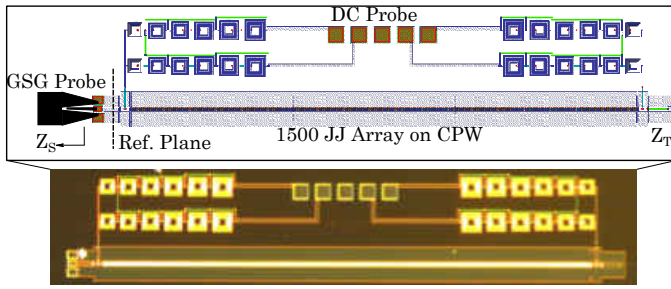
937

Fig. 4. The layout (top) and photo (bottom) of the comb generator chip. The total length of the array $l = 3.25$ mm on the 350 μm thick silicon substrate ($\epsilon_r = 12$) satisfies the lumped-element limit $l < \lambda/8$ for frequencies up to 5 GHz. The CPW consists of a 16 μm wide center conductor with an 8 μm gap to fulfill the 50 Ω requirement.

non-linear term is now better understood as JJ pulses b_1^{pp} propagating towards the generator.

IV. CHIP LAYOUT AND MEASUREMENT PROCEDURE

The layout (top) and photo (bottom) of the JJ comb generator chip are shown in Fig. 4. The chip is fabricated with niobium superconducting electrodes and $\text{Nb}_x\text{Si}_{1-x}$ normal-metal barriers described in detail in [14]. The 1500 junctions are embedded in a superconducting copalanar waveguide (CPW) line with Nb signal and ground conductors on an oxidized silicon substrate. The characteristic impedance is designed to be $50\,\Omega$ and the line is terminated with an on-chip resistor. The array of series-connected junctions consists of 500 vertical stacks of 3 JJs distributed along the central conductor of the CPW with one stack every $6.5\,\mu$m, which implies that each stack can be treated as a lumped-element circuit for the relevant measurement frequencies below 50 GHz.

The circuit is probed with a $150\,\mu$m pitch ground-signal-ground (GSG) probe with a cryogenic probe station. The temperature of the chip is set to 4 K. The critical current is temperature dependent; at 4 K we determined that $I_C = 13.9$ mA and $R_n = 3.8$ mΩ based on measurements of the dc current-voltage characteristics [7]. As in the simulation setup, the spiral-inductor coils are used for dc and low-frequency biasing and measurements along with a 5-pin dc probe.

A two-tier wave-parameter calibration of the LSNA was performed to move the reference plane of the measurements to the input of the JJ array [11], as in Fig. 4. For the first tier, we performed a two-port Short-Open-Load-Thru (SOLT) calibration at the plane of the room-temperature inputs to the cryogenic probe station. At the same plane, we also performed an absolute power and cross-frequency phase calibrations using a power meter and a commercial comb generator, respectively. The second tier calibration used on-chip superconducting calibration structures to perform a Multiline Thru-Reflect-Line calibration, renormalizing the obtained reference impedance to $50\,\Omega$. The frequency grid for the calibration was from 1.25 GHz to 50 GHz with a 1.25 GHz step. We also set the LSNA noise floor to –110 dBm by choosing a 10 Hz intermediate frequency bandwidth.
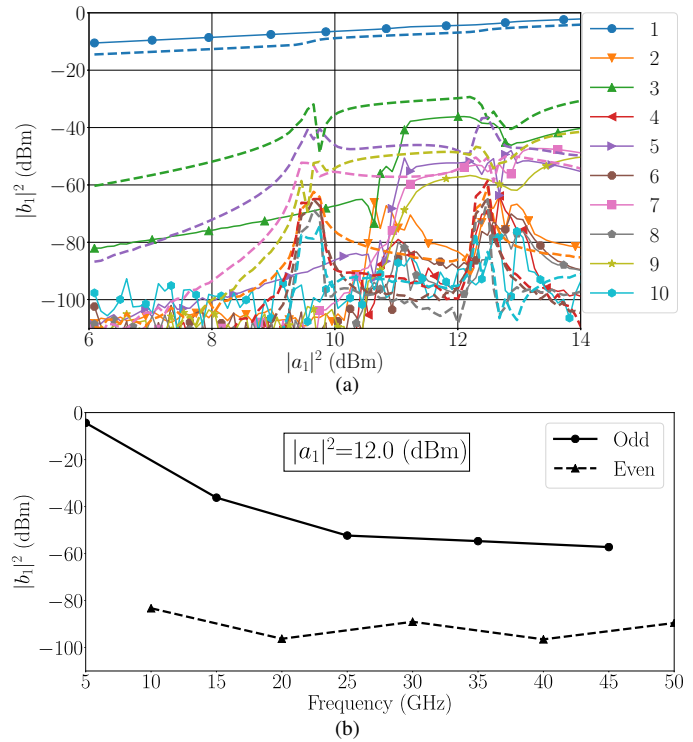

(a)

(b)

Fig. 5. Pulse power: (a) The measured (solid, with markers) and simulated (dashed, no markers) power of the harmonics in the pulses traveling towards the source versus the power of the incident 5 GHz drive signal. The even simulated harmonics are also small and therefore not shown. (b) The measured power of the harmonics versus frequency for a 12 dBm input power.

V. MEASURED AND SIMULATED RESULTS

To demonstrate the performance of our comb generator, we first test the change in output power as a function of input drive amplitude. We follow [3] and first focus on the generation of symmetric pulses. As in Fig. 2, a 5 GHz CW input drive signal from the LSNA and no dc bias are applied to the array. The input drive signal power is swept from 6 dBm to 14 dBm at the reference plane.

The measured and simulated results are shown in Fig. 5, where it is clear that the fundamental component of the b_1-wave has the mismatch term, b_1^{mm}, which dominates. Based on the lowest input power levels, we determine that the return loss of the circuit at the fundamental frequency is 16.6 dB. For the second and third harmonics, non-zero b_1^{nl} components exist for the input power less than about 10.5 dBm due to the small-signal non-linearity of the junctions. For the third and higher-order odd harmonics, note a QLR between 11.2 dBm and 12.1 dBm where the pulse component b_1^{pp} dominates, as in Fig. 2. As expected for symmetrical pulses in this range, the even harmonics are suppressed by greater than 30 dB relative to the neighboring odd harmonics. Within the QLR, the third harmonic at 15 GHz varies by 0.2 dB per 0.1 dB change in the input power. The variation increases with frequency, and the ninth harmonic at 45 GHz varies by 0.5 dB per 0.1 dB change in the input power. Above an input power of about 13 dBm we also begin to observe the generation of two pulses per half-period of the drive signal.
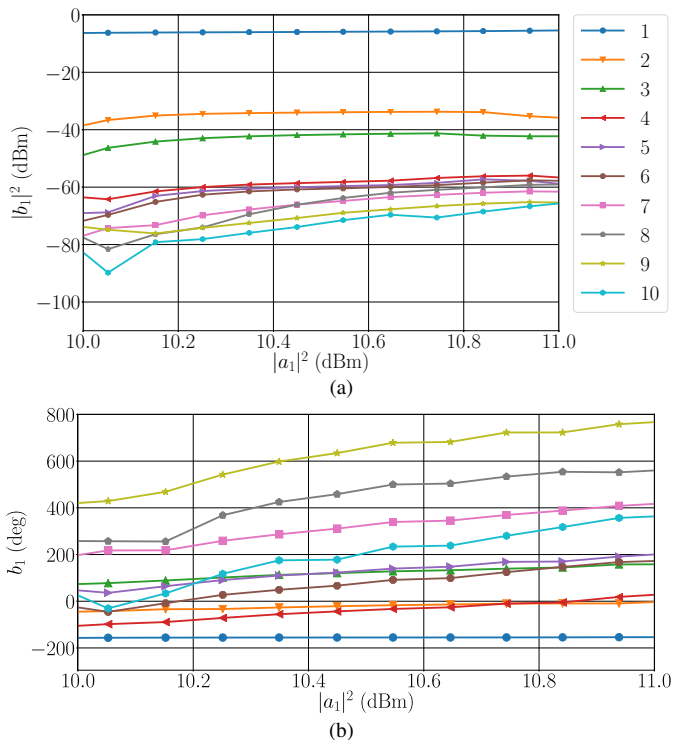
938

Fig. 6. The measured power (a) and phase (b) of the harmonics in the pulses traveling towards the source with a positive dc bias and a 5 GHz CW input drive. The phases of the harmonics are normalized to that of the fundamental component of the incident wave a_1 [1].

We have identified two main simplifications in the model which lead to the differences between the simulations and measurements. First, the differences in the nonlinear small-signal response likely occur because the JJs do not follow a simple sinusoidal dc Josephson equation and instead have a more complicated dependence on ϕ [15]. Second, fabrication tolerances cause variations in the I_c and R_n values of the JJs within the array which is not yet included in our model. The JJ non-uniformity is likely why the simulated QLR is wider than the measured QLR and why the simulated QLR starts at 1 dB smaller input drive power.

Finally, we show the measured power and phase spectra versus input signal amplitude in Fig. 6, where we apply a positive 4 mA dc bias so that only positive pulses are generated. The same level of the power spectrum variation is seen as for the case of symmetric pulses. There is a linear trend in the phase variation and the slope increases with increasing harmonic number n. Specifically, we observe an approximate slope of $8.5 + 4.5(n - 2)$ degrees per 0.1 dB increase in input amplitude. This trend was consistently obtained in several consecutive measurements.

VI. CONCLUSION

In this paper, we show the characterization of a JJ comb generator that generates stable pulses with a predictable harmonic content. We also compare the power of the measured harmonics to simulations involving a simple JJ model, explain the input drive amplitude dependence observed in the measurements, and discuss how the model can be improved. Finally, we achieve an amplitude stability versus input drive variation comparable to that in [6]. Future work will be devoted to more accurately simulating the JJ arrays, accounting for the mismatch term in the fundamental component, investigating in more detail the phase spectrum, characterizing a two-port JJ comb generator, increasing the pulse amplitude by increasing the number of JJs in the array, and improving the comb frequency response by increasing the cutoff frequency of the individual JJ. We will also address the cases of lower-frequency drive signals and thus lower pulse repetition frequencies in future measurements.

REFERENCES

[1] J. Verspecht, "Large-signal network analysis," *IEEE Microwave Magazine*, vol. 6, no. 4, pp. 82–92, Dec 2005.

[2] R. A. Ginley, "Traceability for microwave power measurements: Past, present, and future," in *2015 IEEE 16th Annual Wireless and Microwave Technology Conference (WAMICON)*, April 2015, pp. 1–5.

[3] D. B. Gunyan and J. B. Scott, "Pulse generator," U.S. Patent 7 423 470B2, Sep. 9, 2008.

[4] M. J. W. Rodwell, D. M. Bloom, and B. A. Auld, "Nonlinear transmission line for picosecond pulse compression and broadband phase modulation," *Electronics Letters*, vol. 23, no. 3, pp. 109–110, January 1987.

[5] H. T. Friis, "Analysis of harmonic generator circuits for step recovery diodes," *Proceedings of the IEEE*, vol. 55, no. 7, pp. 1192–1194, July 1967.

[6] H. C. Reader, D. F. Williams, P. D. Hale, and T. S. Clement, "Comb-generator characterization," *IEEE Trans. Microw. Theory Techn.*, vol. 56, no. 2, pp. 515–521, Feb 2008.

[7] T. V. Duzer and C. W. Turner, *Principles of Superconductive Devices and Circuits*, 2nd ed. Upper Saddle River, N.J: Prentice Hall PTR, 1999, ch. 4.

[8] C. J. Burroughs *et al.*, "NIST 10 V programmable josephson voltage standard system," *IEEE Trans. Instrum. Meas.*, vol. 60, no. 7, pp. 2482–2488, July 2011.

[9] N. E. Flowers-Jacobs *et al.*, "Two-volt Josephson arbitrary waveform synthesizer using Wilkinson dividers," *IEEE Trans. Appl. Supercond.*, vol. 26, no. 6, pp. 1–7, Sep. 2016.

[10] P. Solinas, S. Gasparinetti, D. Golubev, and F. Giazotto, "A Josephson radiation comb generator," *Nature Scientific Reports*, vol. 5, no. 12260, pp. 1244–1245, 2015.

[11] A. S. Boaventura *et al.*, "Microwave modeling and characterization of superconductive circuits for quantum voltage standard applications at 4 K," *IEEE Transactions on Applied Superconductivity*, vol. 30, no. 2, pp. 1–7, Mar. 2020.

[12] WRspice Circuit Simulations. Whiteley Res. Sunnyvale, CA, US. [Online]. Available: http://wrcad.com

[13] D. Williams, "Traveling waves and power waves: Building a solid foundation for microwave circuit theory," *IEEE Microw. Mag.*, vol. 14, no. 7, pp. 38–45, Nov 2013.

[14] B. Baek, P. D. Dresselhaus, and S. P. Benz, "Co-sputtered amorphous Nb$_x$ Si$_{1-x}$ barriers for josephson-junction circuits," *IEEE Trans. Appl. Supercond.*, vol. 16, no. 4, pp. 1966–1970, Dec 2006.

[15] A. A. Golubov, M. Y. Kupriyanov, and E. Il'ichev, "The current-phase relation in josephson junctions," *Rev. Mod. Phys.*, vol. 76, pp. 411–469, Apr 2004. [Online]. Available: https://link.aps.org/doi/10.1103/RevModPhys.76.411